IMAGE QUALITY IMPROVEMENTS WITH TIME-OF-FLIGHT POSITRON EMISSION TOMOGRAPHY FOR MOLECULAR IMAGING

Ravindra M. Manjeshwar, Yiping Shao and Floris P Jansen

Functional Imaging, GE Global Research Center, Niskayuna, NY 12309

ABSTRACT

The renewed interest in Time Of Flight (TOF) PET is being driven by the development of detector technology and the growth of new molecular imaging applications. In this study we performed Monte Carlo simulations to quantify image quality improvements as a function of timing resolution for imaging scenarios that mimic whole body and brain imaging. We implemented an iterative image reconstruction algorithm that incorporated time-of-flight information. Image quality, as measured through contrast and noise metrics, consistently improved with improved timing resolution. We simulated and compared a conventional PET scanner with a TOF-PET scanner with 200 ps timing resolution. For lesions embedded in 40cm and 20 cm cylindrical objects, lesion contrast improved by a factor of 3.4 and 2.3, respectively. TOF–PET holds the potential for significantly improved imaging over conventional PET scanners of equivalent sensitivity.

1. INTRODUCTION

Positron **E**mission **T**omography (PET) is a powerful modality to image and quantify physiological and biological processes. Short-lived positron emitting radioisotopes bound to molecular probes are injected into the patient. The distribution of the probe inside the patient depends on the physiological function the probe is designed to track. Inside the patient, an emitted positron interacts with an electron to generate two 511 keV photons in opposite directions. A conventional PET scanner detects this pair of photons and generates an image of the radioisotope distribution by tomographic reconstruction techniques **[1]**.

It has been recognized for some time now, that if the detection of the photon pair was augmented with accurate information on the difference in their arrival times, the position of each emission event could be constrained to a point rather than a line **[2]**. This method, known as Time Of Flight (TOF) PET, reduces the statistical noise in reconstructed images since the region where noise propagates during the reconstruction is restricted. The expected improvement in noise performance makes TOF-PET attractive. This is particularly true for new molecular imaging agents that result in highly specific binding but present a severely count starved imaging situation.

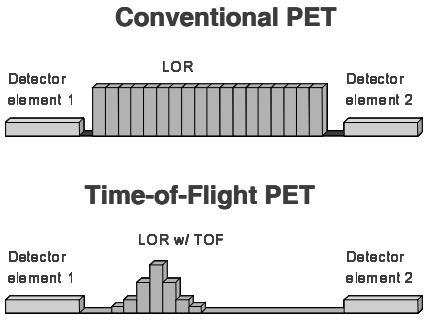

Figure 1: Conventional PET: an event can be uniformly localized to a line between the detectors. Time-of-Flight PET: an event can be probabilistically localized to a short line segment.

In a TOF-PET scanner, the position of the emission event is determined from

$$x = c(t_1 - t_2)/2 \qquad [1]$$

where, t_1 and t_2 are the arrival times of the two photons and c is the speed of light. In reality, TOF information can only be measured within a certain uncertainty dictated by the timing resolution of the detectors. Consequently, the emission event can be localized probabilistically to a short line segment (Fig 1). The uncertainty in event localization is given by

$$\Delta x = c\Delta t/2 \qquad [2]$$

where Δx is the location uncertainty and Δt is the timing resolution. Image quality is expected to improve due to the improved ability to localize the emission event. Additionally, the promised improvements in image quality can be realized only if the size of the object being imaged is greater than the location uncertainty, Δx **[3]**.

In this paper we performed Monte Carlo simulations to study the improvement in image quality as a function of timing resolution. We simulated acquisitions of large and small cylindrical objects to mimic whole body and brain imaging scenarios, respectively. In section 2, an iterative

TOF image reconstruction algorithm and our simulations are described. The results of our analysis are presented in Section 3. The implications of our results for molecular imaging are briefly discussed in Section 4.

2. METHODS

2.1. TOF Reconstruction Algorithm

Reconstruction algorithms based on maximum-likelihood expectation maximization, and specifically the Ordered Subsets Expectation Maximization algorithm, are extensively used in PET imaging [**4,5**]. We implemented the OSEM algorithm incorporating the Time-Of-Flight information.

We considered the following discretized PET model. The detected coincidence data, y_i is the number of detected coincidences along the i^{th} line-of-response (LOR). In a conventional PET scanner, the $\boldsymbol{I}$ LORs are organized by radial $(\boldsymbol{r})$ and angular $(\boldsymbol{\theta})$ co-ordinates. In a TOF-PET scanner, the coincidence data, y_{it} are organized with the additional dimension, $\boldsymbol{t}$, to represent the difference in the detection times of the two photons. Additionally, y_i and y_{it} are related by the following expression.

$$y_i = \sum_t y_{it} \qquad [3]$$

The $N \times N$ pixel square image to be reconstructed is represented as a vector of $\boldsymbol{J}$ (= $N \times N$) pixels. $\boldsymbol{F_j}$ represents the number of emission events from the j^{th} pixel. The system matrix

The iterative update equation for the OSEM algorithm for conventional PET is given by

$$F_j^{k+1} = \frac{F_j^k}{\sum_i P_{ij}} \sum_i P_{ij} \frac{Y_i}{\sum_{j'} P_{ij'} F_j^k} \qquad [4]$$

where P_{ij} is the probability that the emission event from the j^{th} pixel was detected along the i^{th} LOR. The iterative update equation for TOF-PET is

$$F_j^{k+1} = \frac{F_j^k}{\sum_{i,t} P_{ijt}} \sum_{i,t} P_{ijt} \frac{Y_{it}}{\sum_{j'} P_{ij't} F_j^k} \qquad [5]$$

where P_{ijt} is the probability that the emission event from the j^{th} pixel was detected along the i^{th} LOR and in the t^{th} time bin. P_{ij} and P_{ijt} are related by the following expression

$$P_{ijt} = p(j|t,i) P_{ij} \qquad [6]$$

where $p(j|t,i)$ is the probability distribution function which describes the location uncertainty along the i^{th} LOR for the t^{th} time bin.

Equations 4 and 5 describe the update equation for Poisson distributed data. However the coincidence events recorded in a PET scanner are contaminated by "*bad*" coincidence counts called scatter and random coincidences. In addition, the true coincidence counts are attenuated by the material in the object that they pass through. Correcting the measured coincidence counts for random, scatter and attenuation prior to image reconstruction causes significant deviations from the Poisson assumptions of Eqns 4 and 5 leading to degradation in image quality [**6**].

To preserve the Poisson nature of the measured data, we apply the corrections during the reconstruction by modifying Eqns 4 and 5 as follows

$$F_j^{k+1} = \frac{F_j^k}{\sum_i A_i P_{ij}} \sum_i A_i P_{ij} \frac{Y_i}{\sum_{j'} P_{ij'} F_j^k + R_i + S_i} \qquad [6]$$

$$F_j^{k+1} = \frac{F_j^k}{\sum_{i,t} A_i P_{ijt}} \sum_{i,t} a_i P_{ijt} \frac{Y_{it}}{\sum_{j'} P_{ij't} F_j^k + R_{it} + S_{it}} \qquad [7]$$

where A_i are the attenuation correction factors, R_i and S_i are the estimates of the randoms and scatter coincidences for the conventional PET scanner and R_{it} and S_{it} are the randoms and scatter coincidences for the TOF-PET scanner. Of the three corrections, the largest contributing factor for deviations from the Poisson distribution is the attenuation correction. Subtractive correction of randoms and scatter coincidences cannot be ignored as they can result in negative coincidences. This problem is more severe for TOF-PET data, since the total coincidences along a LOR are split into multiple time bins. This results in a lower average number of events per bin, and in consequence proportionately greater statistical variance in counts. The probability of having bins with counts less than the average scatter or randoms signal to be subtracted will therefore increase.

2.2. Simulations

Monte Carlo simulations were performed using SimSET [**7**]for photon transport inside the object being scanned and PSM, a proprietary detector and system modeling code [**8**], to simulate the PET system. We simulated a PET scanner with 4 rings of 70 detector blocks each. Each block had a 9x6 arrangement of 4.25 x 6.25 x 30 mm scintillator crystals. The timing resolution of a TOF-PET scanner is determined from the analog timing resolution of the detector and the least significant bit (LSB) used to digitize the photon detection time. The LSB also determines the number of sinogram time bins required to cover a particular scan field of view. The timing uncertainty was modeled to be Gaussian distributed with the Full-Width-Half-Maximum (FWHM) equal to the timing resolution. We simulated 5-minute acquisitions of digital phantoms with the following timing

resolutions, LSB of the digital time stamps and sinogram sizes.

	Timing resolution (ps)	Time Stamp LSB (ps)	Sinogram Size (r, θ, t)
1	200	100	303 x 315 x 61
2	300	150	303 x 315 x 41
3	500	250	303 x 315 x 25
4	800	400	303 x 315 x 15
5	1000	500	303 x 315 x 13
6	1500	750	303 x 315 x 9
7	NON-TOF	1000	303 x 315 x 1

To separate the effects of detector sensitivities, resolution and random coincidence rates from TOF, all the scanners were assumed to have the same detector scintillator, system sensitivity and randoms coincidence rates.

To simulate large and small objects encountered in whole body and brain imaging we used digital representations of 20 cm long cylinders of 40 and 20 cm diameters, respectively. Each cylinder had three spherical lesions of 5, 10 and 20 mm diameters. The lesions were located 10 cm and 5 cm from the center of the large and small cylinder, respectively. The cylinders were assumed to be filled with water with activity concentration of 0.25 μCi/cc. The lesions had activity concentrations of 1.0 μCi/cc, giving source to background ratios of 4:1.

The simulations produced sinograms for true, scatter and random coincidences. The scatter fractions (ratio of scatter coincidences to sum of the true and scatter coincidences) were 52% and 37% for the 40 and 20 cm cylinders, respectively. These scatter fractions are consistent with scatter fractions observed in septa-less imaging. The random coincidences inside the object were 50% of the total true coincidences. The three sinograms were added together to give the prompts sinogram, which is the raw data that is measured in a scanner.

Images were reconstructed with up to 10 iterations of the TOF–ML–OSEM algorithm with 9 subsets distributed over the 315 trans-axial angles. Images were reconstructed on a 450 mm Field-Of-View (FOV) with a 256x256 pixel grid. To correct the data for random coincidences, the mean randoms rate was estimated using the randoms from singles technique [**9**]. The mean scatter estimate was computed using a model based scatter estimation technique that accounted for TOF information [**10**].

3. RESULTS

Two figures of merit were used to quantify image quality – the percent contrast recovery and the percent background variability. Regions-of-interest with a size equal to that of the lesions were drawn on the lesions. A 5 cm diameter background ROI was drawn at the center of the cylinder. The contrast recovery for each lesion was computed from

$$CR = 100 * \left(C_{lesion} / C_{bkg} - 1 \right) / \left(SBR - 1 \right) \qquad [8]$$

where C_{lesion} and C_{bkg} are the mean counts inside lesion and background ROIs, respectively and SBR is the original source-to-background ratio in the phantom. The percent background variability was computed as the pixel-to-pixel noise standard deviation, normalized by the mean counts inside the background ROI. At each iteration, the contrast recovery and background variability were measured resulting in a C/N curve for each scan. A typical set of C/N curves are shown in Figure 2.

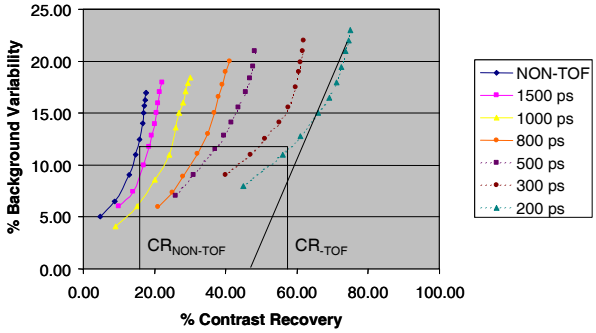

Figure 2: Contrast-Noise curves for 10 mm lesion in 40 cm diameter cylinder.

It can be observed from the C/N curves, that the addition of TOF information improves image quality, as the C/N curves for images with better timing resolution show greater contrast recovery and lower background variability. In addition, greater contrast at the same number of iterations indicates faster convergence with improved timing resolution.

We compared lesion contrasts at equivalent noise levels to quantify the improvements in image quality with TOF-PET. The ratio of percent contrast recovery with and without TOF ($CR_{TOF}/CR_{NON\text{-}TOF}$) was computed at ten noise levels. The noise levels were distributed evenly over a range supported by data in both the TOF and NON-TOF curves. Specifically, the maximum noise level for all comparisons was the noise level at the 10th iteration of NON-TOF. The minimum noise level was chosen as the higher of the noise levels, at the 1st iteration, between the TOF and NON-TOF curves. To extract the percent contrast recovery values at each noise level, the TOF and NON-TOF curves are treated as piece-wise linear between measurements. The mean and standard deviation of the 10 measurements are plotted as function of timing resolution in Figure 3.

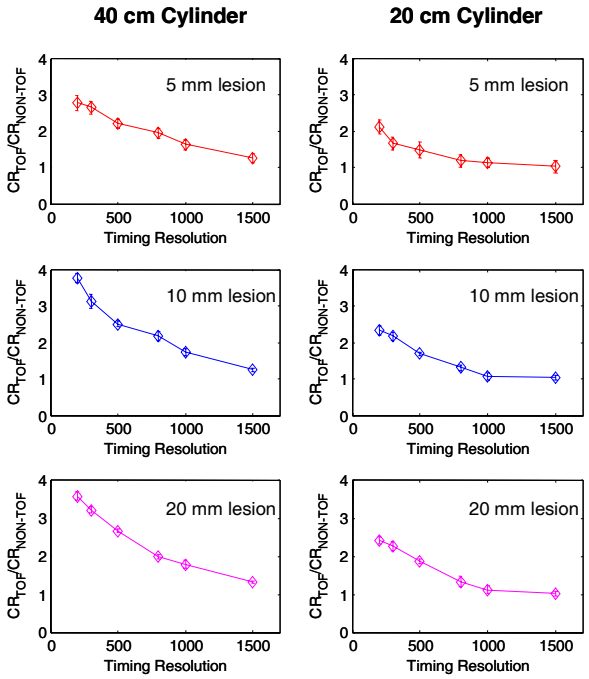

Figure 3: Contrast recovery improvements for TOF-PET with respect to conventional PET

The following observations can be made

i. Lesion contrast improves monotonically with improved timing resolution

ii. Improvements are dependent on the size of the object being imaged, with larger objects showing bigger gains.

iii. Equivalent improvements in lesion contrast with TOF-PET were observed for the 10 mm and 20 mm lesion for both object sizes. In comparison, the 5 mm lesion showed smaller improvements. This is presumably because of the partial volume effect which affects smaller lesions more severely, and needs to be further investigated.

4. DISCUSSION AND CONCLUSIONS

PET imaging is considered one of the more sensitive functional imaging techniques. Despite this, image noise due to the quantum-limited nature of this modality has restricted image quality. The large improvements in image signal-to-noise with TOF-PET will open several opportunities. For oncology applications, the limit of lesion detectability is currently about 10 mm. The approximately 3x improvement in signal-to-noise ratios estimated here with TOF-PET, makes the detection of smaller lesions feasible, leading to earlier detection of disease. The benefits of TOFPET can also be exploited in other ways. For example, the improved noise with TOF-PET can be traded for lower patient dose through smaller injections of the radio-active tracer. It can be traded for shorter acquisition times to improve patient throughput.

Dynamic imaging, where multiple short-acquisition-time images are acquired over extended time periods to study tracer kinetics and function, is a particular application where TOF-PET can have a significant impact. Owing to the short acquisition times, the relatively high noise in the dynamic images poses a challenge for accurate quantitation. As demonstrated, a 200 ps TOF-PET scanner can improve image signal-to-noise by as much as 300% and should allow much-improved quantitation in dynamic images.

We have demonstrated the improvements in lesion contrast with the incorporation of time-of-flight. Lesion contrast improved consistently with detector timing resolution. We believe that development of PET systems with significantly better timing resolution will give a significant boost to the development and success of new molecular imaging applications.

5. REFERENCES

[1] J. A Sorenson and M. E. Phelps, “Physics in Nuclear Medicine”, Second Edition, W. B. Saunders Company, 1987

[2] D. L. Snyder, L. J. Thomas, and M. M. Ter-Pogossian, “A mathematical model for positron-emission tomography systems having time-of-flight measurements,” *IEEE Trans. Nucl. Sci.*, vol. NS-28, pp. 3575–3583, June 1981.

[3] W. W. Moses, “Time of flight in PET revisited,” *IEEE Trans. Nucl. Sci.*, vol. 50, pp. 1325-1330, October 2003.

[4] L. Shepp and Y. Vardi, “Maximum likelihood reconstruction for emission tomography,” *IEEE Trans. Med. Imag.*, vol. MI-1, pp. 113–122, Oct. 1982.

[5] H. Hudson and R. Larkin, “Accelerated image reconstruction using ordered subsets of projection data,” *IEEE Trans. Med. Imag.*, vol. 13, pp. 601–609, Dec. 1994.

[6] M. Iatrou, S.G Ross, R,M. Manjeshwar and C.W Stearns, " A fully 3D iterative image reconstruction algorithm incorporating data corrections", *IEEE Nuclear Science Symposium Conference Record*, Oct 2004.

[7] R.L. Harrison, S.D. Vannoy, D.R Haynor, S.B. Gillispie, M.S. Kaplan, and T.K. Lewellen, “Preliminary Expcricnce with the Photon History Gcnerator Module of a Public- Domain Simulation System Cor Emission Tomography”, *IEEE Nuclear Science Symposium Conference Record*, 1154-1158, 1993.

[8] Y. Shao, R.M. Manjeshwar, F. Jansen and P.Kumar, “PSM: A PET System Modeling capable of generating images with clinically relevant count density. IEEE-MIC, 2003, pp M11-191

[9] C.W Stearns, D.L. McDaniel, S.G Kohlmyer, P.R. Arul, B.P. Geiser and V. Shanmugam, “Random coincidence estimation from single event rates on the Discovery ST PET/CT scanner”, *IEEE Nuclear Science Symposium Conference Record*, Vol 5, Oct. 2003.

[10] S. D. Wollenweber,"Parameterization of a Model-Based 3D PET Scatter Correction", IEEE Transactions in Nuclear Science, vol. 49, no. 3, June 2002.